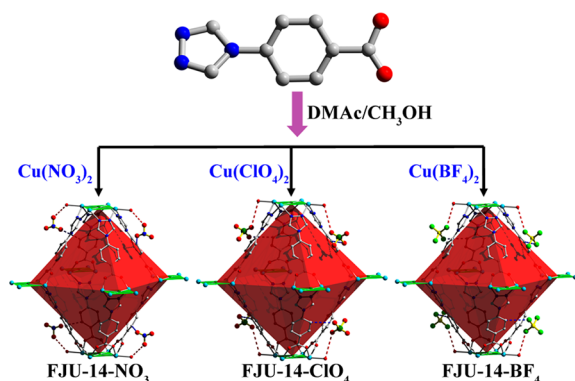


including zeolites,⁵ activated carbons (or carbon nanotubes),⁶ and metal–organic frameworks (MOFs).^{7,8}

Compared with the other solid porous adsorbent materials, the emerging porous metal–organic frameworks received great attention recently, due to their extraordinary surface area,⁹ finely tunable pore surface properties,¹⁰ and ubiquitous potential applications,¹¹ such as gas storage and selective separation,¹² chemical sensing,¹³ proton conductors,¹⁴ and heterogeneous catalysis.¹⁵ In addition, several strategies based on tuning the open metal sites (OMS), polarizing functional groups (Lewis basic sites = LBS), pore size exclusive effect, and flexible framework backbone have been proposed, demonstrating that MOF materials are very promising for postcombustion gas separation and purification.¹⁶ However, there is still a big weakness for most of the porous MOFs, which are likely to disintegrate or shrink into nonporous frameworks after removal of the guest molecules. It is well known that formed rigid nodes and ligands, interpenetrated frameworks, and highly connected metal ion clusters (also known as secondary building units (SBUs)) have been proved as effective methods to preserve the pores and avoid structural collapse.¹⁷ Moreover, supercritical CO₂ activation, freeze-drying treatment, and liquid-solvent exchange have been certified as other effective methods to stabilize the robustness of the porous frameworks during activation.¹⁸ For the nonrobust MOFs, two novel ideas, inserting neutral pillars¹⁹ and introducing large cationic guests,²⁰ have been recently proposed to sustain MOF robustness with tunable porosity, but these methods would reduce the pore volume. To date, improving the MOFs robustness by the balanced multiple hydrogen-bonding interactions (MHBIs) between the host and the guest counteranions has not been observed.

In this article, three isostructural cationic metal–organic frameworks, $\{[(\text{Cu}_4\text{Cl})(\text{cpt})_4(\text{H}_2\text{O})_4]\cdot 3\text{X}\cdot 4\text{DMAC}\cdot \text{CH}_3\text{OH}\cdot 5\text{H}_2\text{O}\}$ (FJU-14, X = NO₃, ClO₄ and BF₄), have been synthesized from bifunctional organic ligands 4-(4*H*-1,2,4-triazol-4-yl) benzoic acid (Hcpt) and various copper salts (Scheme 1) based on considering two aspects. (1) These

Scheme 1. Schematic Diagram for the Synthesis of Three Isostructural Metal Organic Frameworks (MOFs) by Making Use of Different Copper Salts



anions with the different configuration and electronegativity within the channels may bring the MOFs with controllable structure flexibility and robustness due to their distinct interactions between the host and the anions. In comparison with the methods mentioned above to sustain the nonrobust MOFs,^{19,20} as the sizes for these anions are close,²¹ the anion

substitution here will not obviously reduce the pore volume. (2) These anions can provide different polar groups, especially F atoms, to capture CO₂ molecules in conjunction with the skeleton. Interestingly, in contrast with the other two isostructural MOFs, the FJU-14-BF₄ containing BF₄[−] anion in its tetrahedral cages exhibits improved robustness and thermal stability, high uptake, and low-enthalpy CO₂ adsorption. The trapped CO₂ density of 0.955 g cm^{−3} is the highest value among the reported MOFs. The single-crystal structure of its guest-free sample shows that the balanced MHBIs between the BF₄[−] counteranion and the cationic skeleton play a crucial role in stabilizing its framework robustness. Furthermore, single-crystal X-ray diffraction for CO₂ loaded FJU-14-BF₄-a sample shows that CO₂ capture can come from the multiple-point interactions between the adsorbate molecules and the framework as well as its counteranions. Dynamic fixed bed breakthrough experiments indicate that the separation of CO₂/N₂ mixture gases through a column packed with FJU-14-BF₄-a solid can be efficiently achieved.

EXPERIMENTAL SECTION

Materials and Methods. Cu(ClO₄)₂·6H₂O and Cu(BF₄)₂·6H₂O were purchased from J&K Chemical Co., Ltd. and Cu(NO₃)₂·3H₂O, *N,N*-dimethylacetamide (DMAC), and other reagents were purchased from Shanghai Chemical Reagent Co. and used as received without further purification. The ligand Hcpt was prepared according to a known modified method.²² Powder X-ray diffraction (PXRD) was carried out with a PANalytical X'Pert³ powder diffractometer equipped with a Cu-sealed tube ($\lambda = 1.541874 \text{ \AA}$) at 40 kV and 40 mA over the 2θ range of 5–30°. The simulated pattern was produced using the Mercury V1.4 program and single-crystal diffraction data. The Fourier transform infrared (KBr pellets) spectra were recorded in the range of 500–4000 cm^{−1} on a Thermo Nicolet 5700 FT-IR instruments. Thermal analysis was carried out on a METTLER TGA/SDTA 851 thermal analyzer from 30 to 600 °C at a heating rate of 10 °C min^{−1} under nitrogen atmosphere. Elemental analyses (C, H, and N) were performed on a PerkinElmer 240C analyzer.

Syntheses. 4-(4*H*-1,2,4-Triazol-4-yl)benzoic Acid (Hcpt). Refluxing a mixture of *N,N*'-dimethylformamide azine dihydrochloride (2 g, 9.33 mmol) and 4-aminobenzoic acid (1.28 g, 9.33 mmol) in 25 mL of *o*-xylene (reaction should be conducted in a fume hood) for 24 h gave a pale yellow solid, which was filtered and washed with EtOH (1 × 10 mL) and Et₂O (1 × 8 mL); yield 1.21 g (69%). Furthermore, the pale yellow solid and water (5 mL) were transferred into a Parr Teflon-lined stainless steel vessel (23.0 mL) and heated to 150 °C for 24 h under autogenous pressure and cooled to room temperature at a rate of 5.0 °C h^{−1}. Colorless rod-shaped crystals of Hcpt suitable for single-crystal X-ray analysis were obtained directly.

$\{[(\text{Cu}_4\text{Cl})(\text{cpt})_4(\text{H}_2\text{O})_4]\cdot 3\text{NO}_3\cdot 4\text{DMAC}\cdot \text{CH}_3\text{OH}\cdot 5\text{H}_2\text{O}\}$ (FJU-14-NO₃). A mixture of Hcpt (19.5 mg, 0.1 mmol) and Cu(NO₃)₂·3H₂O (25.3 mg, 0.1 mmol) was dissolved in 3 mL of DMAC/CH₃OH (2:1, v/v) in a screw-capped vial. After addition of 10 μL of HCl (3 M, aq), the vial was heated at 80 °C for 1 day under autogenous pressure. Green polyhedral crystals were obtained after filtration, washed with CH₃OH, and dried in air. Yield 48% (based on Hcpt). Anal. Calcd for Cu₄ClC₅₃H₈₂N₁₉O₃₁ (1770.98): C, 35.91; H, 4.630; N, 15.02. Found: C, 36.83; H, 4.657; N, 15.05. IR (KBr, cm^{−1}): 3430 (s), 3095 (w), 2919 (w) 1621 (s), 1552 (m), 1386 (s), 1253(w), 1010 (s), 785 (w) cm^{−1}.

$\{[(\text{Cu}_4\text{Cl})(\text{cpt})_4(\text{H}_2\text{O})_4]\cdot 3\text{ClO}_4\cdot 4\text{DMAC}\cdot \text{CH}_3\text{OH}\cdot 5\text{H}_2\text{O}\}$ (FJU-14-ClO₄). The synthetic procedure was similar to that of FJU-14-NO₃ except that Cu(NO₃)₂·3H₂O was replaced by Cu(ClO₄)₂·6H₂O. Green polyhedral crystals were obtained after filtration, washed with CH₃OH, and dried in air. Yield 48% (based on Hcpt). Anal. Calcd for Cu₄Cl₄C₅₃H₈₂N₁₆O₃₄ (1883.32): C, 33.77; H, 4.354; N, 11.89. Found:

C, 34.36; H, 4.541; N, 12.33. IR (KBr, cm^{-1}): 3442 (s), 3106 (w), 1629 (s), 1552 (m), 1382 (s), 1253(w), 1110 (s), 785 (w) cm^{-1} .

[(Cu_4Cl)(cpt) $_4(\text{H}_2\text{O})_4$] $\cdot 3\text{BF}_4 \cdot 4\text{DMAc} \cdot \text{CH}_3\text{OH} \cdot 5\text{H}_2\text{O}$ (FJU-14-BF $_4$). The synthetic procedure was similar to that of FJU-14-NO $_3$ except that $\text{Cu}(\text{NO}_3)_2 \cdot 3\text{H}_2\text{O}$ was replaced by $\text{Cu}(\text{BF}_4)_2 \cdot 6\text{H}_2\text{O}$. Green polyhedral crystals were obtained after filtration, washed with CH_3OH , and dried in air. Yield 42% (based on Hcpt). Anal. Calcd for $\text{C}_{24}\text{ClB}_3\text{F}_{12}\text{C}_{53}\text{H}_{82}\text{N}_{16}\text{O}_{22}$ (1845.38): C, 34.46; H, 4.443; N, 12.14. Found: C, 34.34; H, 4.268; N, 11.84. IR (KBr, cm^{-1}): 3450(s), 2930 (m), 1623 (s), 1550(m), 1415(s), 1257(w), 1080(s), 785 (w) cm^{-1} .

Gas Adsorption. After the bulk of the solvent was decanted, the freshly prepared sample of FJU-14 (~0.15 g) was soaked in methanol for 1 h, and then the solvent was decanted. Following the procedure of methanol soaking and decanting 10 times, the solvent-exchanged samples were activated by vacuum at room temperature for 24 h until a pressure of 5 μm of Hg. N_2 and CO_2 adsorption isotherms were measured on Micromeritics ASAP 2020 HD88 surface area analyzer for the guest-free FJU-14-a. The sorption measurement was maintained at 77 K with liquid nitrogen and at 273 K with an ice-water bath (slush). A water bath was used for adsorption isotherms at 296 K.

Virial Equation Analysis. The virial equation can be written²³ as follows

$$\ln(n/p) = A_0 + A_1n + A_2n^2 + \dots \quad (1)$$

where n is the amount adsorbed (mol g^{-1}) at pressure p (Pa). At a low surface coverage, the A_2 and higher terms can be neglected and the equation becomes

$$\ln(n/p) = A_0 + A_1n \quad (2)$$

A linear graph of $\ln(n/p)$ versus n was obtained at low surface coverage, and this is consistent with neglecting the higher terms in eq 2. A_0 is related to the adsorbate–adsorbent interactions, whereas A_1 describes the adsorbate–adsorbate interactions. The virial parameters are given in Table S3, Supporting Information.

Enthalpies of Adsorption. Zero Surface Coverage. The isosteric enthalpies of adsorption at zero surface coverage ($Q_{st,n=0}$) are a fundamental measure of adsorbate–adsorbent interactions, and these values were calculated from the A_0 values obtained by extrapolation of the virial graph to zero surface coverage.

van't Hoff Isochore. The isosteric enthalpies of adsorption as a function of surface coverage were calculated from the isotherms using the van't Hoff isochore, which is given by the equation

$$\ln(p) = -\frac{\Delta H}{RT} + \frac{\Delta S}{R} \quad (3)$$

A graph of $\ln(p)$ versus $1/T$ at a constant amount adsorbed (n) allows the isosteric enthalpy and entropy of adsorption to be determined. The pressure values for a specific amount adsorbed were calculated from the adsorption isotherms by (1) assuming a linear relationship between the adjacent isotherm points starting from the first isotherm point and (2) using the virial equation at low surface coverage. The agreement between the two methods for FJU-14-BF $_4$ -a are shown in Figure S12.

Column Breakthrough Experiments. The mixed-gas breakthrough separation experiment was conducted at 296 K using a lab-scale fix-bed reactor (Scheme S2). In a typical experiment, ~0.25 g of FJU-14-BF $_4$ powder was packed into a stainless steel column (the steel column was 18 cm in length with a 4 mm inner (6.4 mm outer) diameter) with silica wool filling the void space. The sorbent was activated in situ in the column with a vacuum pump at 296 K for 24 h. A helium flow (5 mL min^{-1}) was used after the activation process to purge the adsorbent. The flow of He was then turned off, while a gas mixture of CO_2/N_2 (15:85, V/V) at 5 mL min^{-1} was allowed to flow into the column. The effluent from the column was monitored using a Hiden mass spectrometer (HPR 20). The complete breakthrough of CO_2 and other species was indicated by the downstream gas composition reaching that of the feed gas. On the basis of the mass balance, the gas adsorption capacities can be determined as follows²⁴

$$q_i = \frac{C_i V}{22.4 \times m} \times \int_0^t \left(1 - \frac{F}{F_0}\right) dt \quad (4)$$

where q_i is the equilibrium adsorption capacity of gas i (mmol g^{-1}), C_i is the feed gas concentration, V is the volumetric feed flow rate ($\text{cm}^3 \text{min}^{-1}$), t is the adsorption time (min), F_0 and F are the inlet and outlet gas molar flow rates, respectively, and m is the mass of the adsorbent (g).

Single-Crystal X-ray Diffraction (SCXRD) Studies. Data collection and structural analysis of crystal FJU-14 were collected on an Agilent Technologies SuperNova single-crystal diffractometer equipped with graphite monochromatic Cu $K\alpha$ radiation ($\lambda = 1.54184 \text{ \AA}$). The crystal was kept at 150 or 100 K during data collection. Using Olex2,²⁵ the structure was solved with the Superflip structure solution program using charge flipping and refined with the ShelXL refinement package using least-squares minimization. The cpt ligand is disordered over two positions (occupancy 0.5:0.5); this is due to the fact that triazolate and the carboxylate part of the ligand show similar coordination models and therefore can substitute each other at the given site. Additionally, the disorder of the triazolate group leads to the carbon and nitrogen atoms sharing the same crystallographic positions with partial occupancies in these compounds. All non-hydrogen atoms were refined with anisotropic displacement parameters. The hydrogen atoms on the ligands were placed in idealized positions and refined using a riding model. Hydrogen atoms for the terminal coordinate water in these compounds were not able to locate as they were found to be disordered. We employed PLATON²⁶ and SQUEEZE²⁷ to calculate the diffraction contribution of the solvent molecules and thereby produce a set of solvent-free diffraction intensities.

SCXRD for CO_2 -Loaded FJU-14-BF $_4$ -a (FJU-14-BF $_4$ -a-0.93 CO_2). The solvent-exchanged single crystal of FJU-14-BF $_4$ was fixed inside a glass capillary and pretreated similarly as for the gas adsorption measurements to get the guest-free FJU-14-BF $_4$ -a. The capillaries were cooled to cryogenic temperature (dry ice–acetone), backfilled with CO_2 (1 atm), and finally sealed by a torch. After that, the CO_2 -loaded single crystal was immediately removed to a dry liquid nitrogen atmosphere (100 K) for structural analysis. The detailed crystallographic data and structure refinement parameters for these compounds are summarized in Table S1, Supporting Information (CCDC 1426056–1426060).

RESULTS AND DISCUSSION

Crystal Structures. Green polyhedral crystals of FJU-14 were solvothermally synthesized by reaction of various copper salts and Hcpt in DMAc– CH_3OH solution for 1 day. Single-crystal X-ray study reveals that FJU-14 crystallizes in the tetragonal space group $I4/mmm$. As shown in Figure 1a, there is one crystallographically independent Cu^{2+} ion, its octahedral geometry completed by four independent cpt ligands, a $\mu_4\text{-Cl}^-$ anion, and one terminal water molecule. The Cl^- anion connects with four Cu^{2+} ions to form $[\text{Cu}_4\text{Cl}]^{7+}$ square plane SBU. There are two types of polyhedral nanocages in FJU-14, that is, one octahedron (Cage A) and one tetrahedron (Cage B) (Figure 1b). Cage A with its center at the Wyckoff position 2b is constructed by six $[\text{Cu}_4\text{Cl}]^{7+}$ SBUs as vertices and eight cpt ligands as the edges. As its equator has no cpt occupied, each triangle face of the octahedron is composed of two cpt edges and three $[\text{Cu}_4\text{Cl}]^{7+}$ vertices. In addition, the dimension of this cage is estimated to be around 14 \AA . Cage B with its center at the Wyckoff position 4d consists of four $[\text{Cu}_4\text{Cl}]^{7+}$ SBUs and four cpt ligands, with a dimension of 5.8 \AA . On the whole, Cage A is linked by eight Cage B through sharing eight triangle faces (Figure S1b). Similarly, Cage B is linked by four Cage A by sharing four triangle faces. The connection of two types of polyhedral nanocages extends to form a three-dimensional (3D) cationic framework (Figure 1c). For the

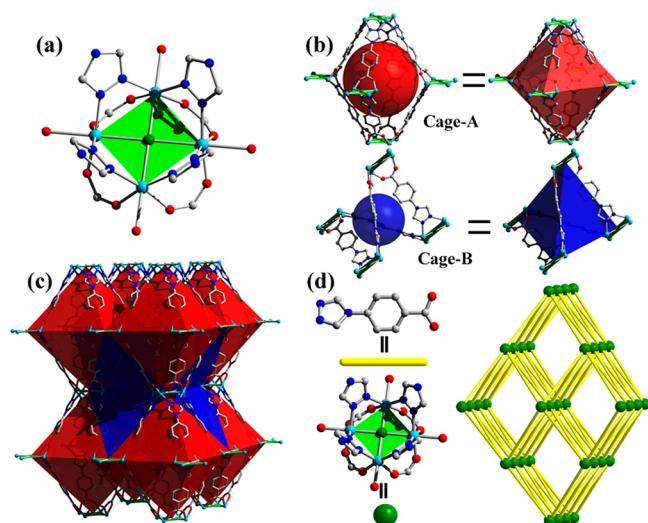


Figure 1. (a) Tetranuclear $[\text{Cu}_4\text{Cl}]^{7+}$ square face SBU in FJU-14. (b) Two types of polyhedral nanocages observed in FJU-14: one octahedral cage (Cage-A, red) and one tetrahedral cage (Cage-B, blue). (c) Face-shared packing of octahedral and tetrahedral cages in FJU-14. (d) Schematic representation of the 8-connected bcu topology in FJU-14. Color code: Cu, sky blue; Cl, green; O, red; C, gray; N, blue (hydrogen atoms are omitted from the structure for clarity).

sake of clarity, if we simplify $[\text{Cu}_4\text{Cl}]^{7+}$ vertices as eight-connected nodes, FJU-14 adopts the bcu network with the topological point symbol of $4^{24}.6^4$ (Figure 1d).²⁸ After elimination of guest solvent molecules, the total accessible volumes in FJU-14- NO_3 , FJU-14- ClO_4 , and FJU-14- BF_4 are 43.1%, 48.7%, and 46.0%, respectively, by using the PLATON software.²⁶ The anion substitution does not obviously decrease the pore volume of FJU-14.

It is worth noting that each tetrahedral cage in FJU-14 is occupied by the counteranions (NO_3^- , ClO_4^- , or BF_4^-) in pair to balance the frameworks' charge. The counteranions provide its own donors D (O or F) to produce multiple $\text{D}\cdots\text{H}-\text{A}$ hydrogen-bonding interactions with acceptors A (phenyl ring or coordinated water molecule). The difference in configuration and electronegativity for these counteranions in the series of MOFs leads to the remarkably distinct MHBIs between the host and the anions (Figure 2a–c). The location for the minor planar NO_3^- ion is much closer to the terminal coordination water ($d[\text{O}(\text{NO}_3^-)\cdots\text{Ow}(\text{H}_2\text{O})] = 2.742 \text{ \AA}$) than to a phenyl ring ($d[\text{O}(\text{NO}_3^-)\cdots\text{C}(\text{phenyl})] = 3.459 \text{ \AA}$). In contrast, the tetrahedral anion, especially BF_4^- containing more electronegative F atoms, can provide balanced MHBIs with the phenyl ring ($d[\text{F}(\text{BF}_4^-)\cdots\text{C}(\text{phenyl})] = 3.133 \text{ \AA}$) and with the coordinated water molecule ($d[\text{F}(\text{BF}_4^-)\cdots\text{Ow}(\text{H}_2\text{O})] = 3.466 \text{ \AA}$).²⁹ The balanced MHBIs between the host and the counteranions may bring better performance to FJU-14- BF_4 .

Robustness and Thermal Stability. The robustness and thermal stability for the three isostructural MOFs were measured by using the powder X-ray diffraction (PXRD) and thermogravimetric analysis (TGA) technologies. From TGA curves, the as-synthesized samples FJU-14- NO_3 and FJU-14- ClO_4 show a similar continuous weight loss upon heating, while the as-synthesized and activated FJU-14- BF_4 shows a plateau up to 270 °C following with a sharp weight loss, indicating the collapse of the frameworks (Figure S5). The PXRD patterns of as-synthesized FJU-14 are coincident with the simulated ones

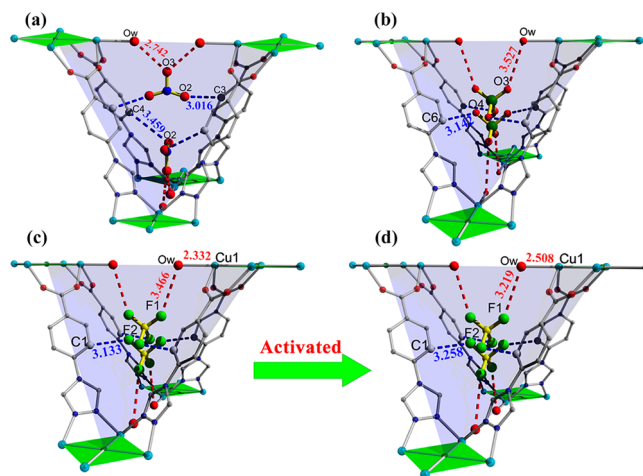


Figure 2. Counteranions (NO_3^- , ClO_4^- , BF_4^-) locate in the tetrahedral cage and show the MHBIs between the counteranions and cationic frameworks in (a) FJU-14- NO_3 , (b) FJU-14- ClO_4 , (c) FJU-14- BF_4 , and (d) the activated FJU-14- BF_4 -a. The counteranion $\cdots\text{H}_2\text{O}$ and counteranion \cdots phenyl ring interactions are indicated as red and blue dashed lines. Sky blue, green, blue, red, gray, yellow, and bright green spheres represent Cu, Cl, N, O, C, B, and F atoms, respectively.

from the single-crystal data, indicative of its high purity and homogeneity (Figures 3, S6, and S7). The variable-temperature PXRD (VT-PXRD) indicates that the framework structure of FJU-14- NO_3 and FJU-14- ClO_4 can be retained at temperatures up to 220 °C without any phase change, while FJU-14- BF_4 is stable even above 250 °C. The balanced MHBIs between the host skeleton and the BF_4^- counteranions bring FJU-14- BF_4 with higher thermally stable temperature. Furthermore, the robustness for desolvated phase of FJU-14 was observed by PXRD after the as-synthesized samples were exchanged with CH_3OH several times and activated at room temperature (RT) for 24 h under high vacuum. The activated FJU-14- NO_3 -a almost loses its crystallinity, while FJU-14- ClO_4 -a still keeps the crystallinity but with several peaks shifting and changing. It indicates that the two MOFs are dynamic and partly shrink or even collapse after the activation.³⁰ On the contrary, the PXRD pattern for the activated FJU-14- BF_4 -a is in good agreement with the as-synthesized one. Besides the improved thermal stability, the balanced MHBIs also endow FJU-14- BF_4 with enhanced robustness, in comparison with the other two MOFs.

Gas Adsorption Studies. The improved robustness and stability by the balanced MHBIs in FJU-14- BF_4 encourage us to further examine the effect of counteranions on the pore structures and CO_2 adsorption for the three MOFs. Their N_2 sorption isotherms at 77 K are shown in Figure 4a. FJU-14- NO_3 -a takes much less N_2 gas with no pore volume. FJU-14- ClO_4 -a exhibits a typical type-IV behavior and the pore condensation with pronounced adsorption–desorption hysteresis, while FJU-14- BF_4 -a shows reversible type-I isotherm and appears to have small hysteretic sorption behavior because of dynamic features and the cage effect.³¹ FJU-14- BF_4 -a has the BET/Langmuir surface area of $324/447 \text{ m}^2 \text{ g}^{-1}$, 5-fold the value (62/90) for FJU-14- ClO_4 -a, although their pore volumes are closed (0.172 vs $0.125 \text{ cm}^3 \text{ g}^{-1}$). By the nonlocal density functional theory (NLDFT) method,³² FJU-14- BF_4 -a shows a bimodal pore-size distribution centering at 5.8 and 8.8 Å (Figure S8). The significantly different pore structures of the

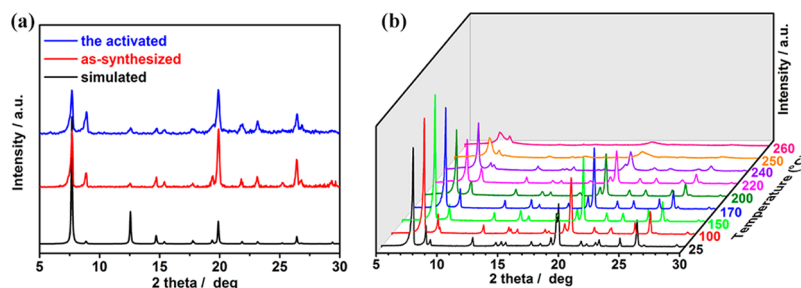


Figure 3. (a) Room-temperature conditions and (b) variable-temperature powder X-ray diffraction patterns for FJU-14-BF₄.

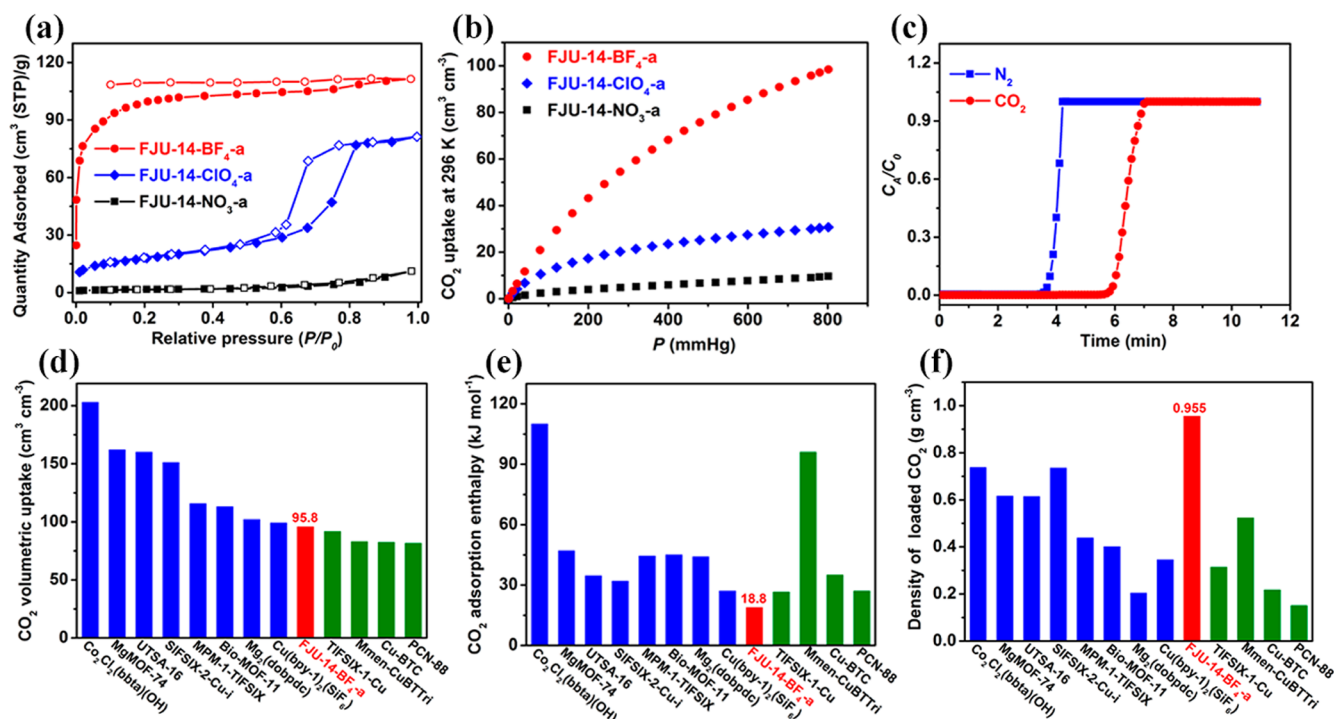


Figure 4. (a) N₂ sorption isotherms of FJU-14-NO₃-a (black), FJU-14-ClO₄-a (blue), and FJU-14-BF₄-a (red) at 77 K. (b) Comparison of CO₂ sorption isotherms of FJU-14-a at 296 K. (c) Column breakthrough experiment for a CO₂/N₂ = 15/85 gas mixture carried out on FJU-14-BF₄-a at 296 K and 1 bar. The flow rate of CO₂/N₂ gas mixture is 5 mL min⁻¹. The comparison of CO₂ uptake (d), adsorption enthalpy (e), and loaded CO₂ density (f) on FJU-14-BF₄-a with representative MOFs. Blue (green) bars represent representative MOFs with the CO₂ volumetric uptake higher (lower) than FJU-14-BF₄-a.

FJU-14 are attributed to the various robustness nature resulted from the MHBIs between the hosts and the guests.

At 296 K and 1 bar, FJU-14-BF₄-a can take CO₂ of 95.8 cm³ cm⁻³ (Figure 4b), three-fold more than that for FJU-14-ClO₄-a (30 cm³ cm⁻³). The virial graphs for CO₂ adsorption on FJU-14-BF₄-a at 273 and 296 K are shown in Figure S11. The comparison of the results from the two methods, the linear extrapolation and the virial equation, shows very good agreement (Figure S12). The enthalpy at zero coverage $Q_{st,n=0}$ for CO₂ adsorption on FJU-14-BF₄-a is 18.8 kJ mol⁻¹, slightly larger than the CO₂ vaporization enthalpy (16.5 kJ mol⁻¹).³³ The amount of absorbed CO₂ in FJU-14-BF₄-a at 296 K is lower than some famous MOFs, such as Co₂Cl₂(bbta)(OH) (203 cm³ cm⁻³),³⁴ MgMOF-74 (162 cm³ cm⁻³),³⁵ UTSA-16 (160 cm³ cm⁻³),³⁶ SIFSIX-2-Cu-i (151 cm³ cm⁻³),³⁷ and is comparable with the values on MPM-1-TIFSIX (115.7 cm³ cm⁻³),³⁸ Bio-MOF-11 (113 cm³ cm⁻³),³⁹ Mg₂(dobpdc) (102 cm³ cm⁻³),⁴⁰ and Mmen-CuBTTri (83 cm³ cm⁻³)⁴¹ (Figure 4d). However, the adsorption enthalpy value of FJU-14-BF₄-a is significantly lower than some representative MOFs

for large CO₂ uptake: Co₂Cl₂(bbta)(OH) (110 kJ mol⁻¹),³⁴ Mmen-CuBTTri (96 kJ mol⁻¹),⁴¹ Mg-MOF-74 (47 kJ mol⁻¹),⁴² Bio-MOF-11 (45 kJ mol⁻¹),³⁹ MPM-1-TIFSIX (44.4 kJ mol⁻¹),³⁸ and Mg₂(dobpdc) (44 kJ mol⁻¹)⁴⁰ (Figure 4e). The CO₂ density in FJU-14-BF₄-a at 1 atm and 296 K is estimated according to the amount of gas adsorbed and the pore volume (0.172 cm³ g⁻¹) of the framework from N₂ adsorption at 77 K. It is 0.955 g cm⁻³, close to the liquid CO₂ density of 1.032 g cm⁻³,⁴³ the highest ever reported on the MOFs for CO₂ capture at the same condition (Figure 4f). The highest CO₂ density means FJU-14-BF₄-a can trap CO₂ in the most efficient mode into its pore to reach saturation even at 296 K and 1 atm, featuring FJU-14-BF₄-a as the very promising material for the highly selective separation of CO₂ from the light gases. The CO₂ uptake on FJU-14-BF₄-a is about 14 times the N₂ uptake (6.9 cm³ cm⁻³) (Figure S9). To evaluate the performance of FJU-14-BF₄-a in the actual adsorption-based separation and purification processes, dynamic column breakthrough experiments were performed in which a CO₂/N₂ (15:85, v/v) mixture was flowed over a packed bed of FJU-

14-BF₄-a solid with a total flow of 5 mL min⁻¹ at 296 K. As shown in Figure 4c, the separation of a CO₂/N₂ (15:85, v/v) mixture through the column packed bed of FJU-14-BF₄-a solid can be efficiently achieved. The dynamic CO₂ adsorption capacity in FJU-14-BF₄-a at room temperature is 0.99 mmol g⁻¹, comparable with the values on MOF-890 (1.38 mmol g⁻¹)⁴⁴ and IRMOF-74-III-CH₂NH₂ (0.8 mmol g⁻¹),⁴⁵ and higher than HKUST-1 (0.45 mmol g⁻¹).⁴⁶

In order to elucidate the mechanism for the high-density CO₂ adsorption on FJU-14-BF₄-a, we employed the single-crystal X-ray diffraction technique to solve the high-quality crystal structures for both the guest-free and the CO₂-loaded FJU-14-BF₄-a samples at low temperature. The single-crystal structure for the guest free sample (Figure 2d) reveals that the bond length of Cu–Ow changes from 2.332 to 2.508 Å; meanwhile, the distance $d[\text{F}(\text{BF}_4^-)\cdots\text{Ow}(\text{H}_2\text{O})]$ is shortened to 3.219 Å, very close to that of $d[\text{F}(\text{BF}_4^-)\cdots\text{C}(\text{phenyl})]$ (3.258 Å). After the activation, the MHBIs between the host and the counteranion BF₄⁻ become more balanced, contrasting to the origin sample. The more balanced MHBIs keep the framework more robust and stable even after the activation. Single-crystal X-ray diffraction analysis of the gas-loaded MOFs has been demonstrated as a straightforward and convincing tool to elucidate the gas adsorption mechanism,⁴⁷ in comparison with other tools including theoretical calculations,⁴⁸ spectroscopy,⁴⁹ and synchrotron powder X-ray diffraction (SPXRD).⁵⁰ The single-crystal structure for the CO₂-loaded sample FJU-14-BF₄-a·0.93CO₂ reveals that it has two crystallographically independent CO₂ molecules (Figure 5): one in an octahedral

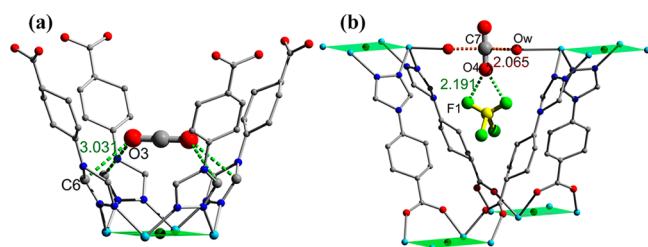


Figure 5. Local environment of FJU-14-BF₄-a·0.93CO₂ showing the multipoint supramolecular interactions (green and orange dashed lines) between the CO₂ molecules (I and II) and the framework as well as its counteranions (a and b).

case (denoted as CO₂-I) and one-half of another in one tetrahedral cage (denoted as CO₂-II). The CO₂ occupancies at the two sites I and II were determined by free structural refinement to be 0.29256 and 0.1744, respectively. The CO₂-I molecule locates near to four 1,2,4-triazolyl rings, with its electronegative O atom interacting with the electropositive C atom of the 1,2,4-triazolyl rings [$\text{O}(\delta^-)\cdots\text{C}(\delta^+) = 3.031 \text{ \AA}$], which is normally considered as the binding domains of CO₂ in MOFs (Tables S5).⁴⁷ The CO₂-II molecule is surrounded with two coordinated water and two BF₄⁻ anions from two edge-sharing tetrahedral cages. This configuration keeps both oxygen atoms of CO₂-II relatively close to the F atoms from the BF₄⁻ anions ($d[\text{O}(\text{CO}_2)\cdots\text{F}(\text{BF}_4^-)] = 2.191 \text{ \AA}$). Further, CO₂-II could interact with the terminal water molecules via the interaction between the Ow lone pair and the C atom of CO₂ ($d[\text{C}(\text{CO}_2)\cdots\text{O}(\text{H}_2\text{O})] = 2.065 \text{ \AA}$). These results indicate that the high-density CO₂ adsorption on FJU-14-BF₄-a with low enthalpy is mainly attributed to the multipoint supramolecular

interactions between CO₂ molecules and the BF₄⁻ anions as well as the host skeleton.

CONCLUSIONS

In summary, we synthesized three isostructural microporous cationic metal–organic frameworks (FJU-14) and first demonstrated that the robustness, stability, and gas separation capacity of the MOFs can be tuned by alerting the weak interactions between the host and the counteranions. Among the three MOFs, FJU-14-BF₄ containing a BF₄⁻ anion in its tetrahedral cages can take CO₂ with a high volume uptake (95.8 cm³ cm⁻³) but low enthalpy (18.8 kJ mol⁻¹) at ambient conditions. The trapped CO₂ density of 0.955 g cm⁻³ is the highest value among the reported MOFs. Dynamic fixed-bed breakthrough experiments indicate that the separation of CO₂/N₂ mixture gases through a column packed with FJU-14-BF₄-a solid can be efficiently achieved. The balanced MHBIs between the BF₄⁻ counteranion and the cationic skeleton play a crucial role in the stability of FJU-14-BF₄-a. The high-density CO₂ capture is mainly contributed from the multiple-point interactions between the adsorbate molecules and the framework as well as its counteranions. We do believe that our findings will encourage further work in the control of multiple hydrogen-bonding interactions for MOFs, especially the nonrobust MOFs, to improve their stability and gas separation capacity through the counterion substitution.

ASSOCIATED CONTENT

Supporting Information

The Supporting Information is available free of charge on the ACS Publications website at DOI: 10.1021/acs.inorgchem.5b02316.

Details of experimental methods and procedures, additional structural figures, FT-IR spectra, TGA curves, PXRD patterns, and gas absorption isotherms (PDF) X-ray crystallographic data (CIF)

AUTHOR INFORMATION

Corresponding Authors

*E-mail: lhwang@fjnu.edu.cn.

*E-mail: scxiang@fjnu.edu.cn.

Notes

The authors declare no competing financial interest.

ACKNOWLEDGMENTS

This work was financially supported by the National Natural Science Foundation of China (21207018, 21273033, 21203024, and 21573042) and the Fujian Science and Technology Department (2014J06003 and 2014H6007). S.X. gratefully acknowledges the support of the Recruitment Program of Global Young Experts, Program for New Century Excellent Talents in University (NCET-10-0108), and the Award “MinJiang Scholar Program” in Fujian Province.

REFERENCES

- (1) WMO. *Greenhouse Gas Bulletin No. 8*; World Meteorological Organization: Geneva, 2012.
- (2) Quadrelli, R.; Peterson, S. *Energy Policy* **2007**, *35*, 5938–5952.
- (3) Haszeldine, R. S. *Science* **2009**, *325*, 1647–1652.
- (4) Rochelle, G. T. *Science* **2009**, *325*, 1652–1654.
- (5) (a) Siriwardane, R. V.; Shen, M. S.; Fisher, E. P. *Energy Fuels* **2005**, *19*, 1153–1159. (b) Chue, K. T.; Kim, J. N.; Yoo, Y. J.; Cho, S.

- H.; Yang, R. T. *Ind. Eng. Chem. Res.* **1995**, *34*, 591–598. (c) Palomino, M.; Corma, A.; Jorda, J. L.; Rey, F.; Valencia, S. *Chem. Commun.* **2012**, *48*, 215–217.
- (6) (a) Drage, T. C.; Blackman, J. M.; Pevida, C.; Snape, C. E. *Energy Fuels* **2009**, *23*, 2790–2796. (b) Mishra, A. K.; Ramaprabhu, S. *Energy Environ. Sci.* **2011**, *4*, 889–895.
- (7) (a) Sumida, K.; Rogow, D. L.; Mason, J. A.; McDonald, T. M.; Bloch, E. D.; Herm, Z. R.; Bae, T. H.; Long, J. R. *Chem. Rev.* **2012**, *112*, 724–781. (b) Li, J. R.; Sculley, J.; Zhou, H. C. *Chem. Rev.* **2012**, *112*, 869–932.
- (8) (a) Banerjee, R.; Furukawa, H.; Britt, D.; Knobler, C.; O’Keefe, M.; Yaghi, O. M. *J. Am. Chem. Soc.* **2009**, *131*, 3875–3877. (b) He, C. T.; Liao, P. Q.; Zhou, D. D.; Wang, B. Y.; Zhang, W. X.; Zhang, J. P.; Chen, X. M. *Chem. Sci.* **2014**, *5*, 4755–4762. (c) Pachfule, P.; Chen, Y.; Sahoo, S. C.; Jiang, J.; Banerjee, R. *Chem. Mater.* **2011**, *23*, 2908–2916. (d) Wang, F.; Fu, H. R.; Kang, Y.; Zhang, J. *Chem. Commun.* **2014**, *50*, 12065–12068. (e) Gao, W. Y.; Pham, T.; Forrest, K. A.; Space, B.; Wojtas, L.; Chen, Y. S.; Ma, S. *Chem. Commun.* **2015**, *51*, 9636–9639.
- (9) Furukawa, H.; Ko, N.; Go, Y. B.; Aratani, N.; Choi, S. B.; Choi, E.; Yazaydin, A. O.; Snurr, R. Q.; O’Keefe, M.; Kim, J.; Yaghi, O. M. *Science* **2010**, *329*, 424–428.
- (10) (a) Rowsell, J. L. C.; Yaghi, O. M. *J. Am. Chem. Soc.* **2006**, *128*, 1304–1315. (b) Wang, Z.; Cohen, S. M. *Chem. Soc. Rev.* **2009**, *38*, 1315–1329.
- (11) (a) Furukawa, H.; Cordova, K. E.; O’Keefe, M.; Yaghi, O. M. *Science* **2013**, *341*, 1230444. (b) Chen, B. L.; Xiang, S. C.; Qian, G. D. *Acc. Chem. Res.* **2010**, *43*, 1115–1124. (c) Qiu, S. L.; Zhu, G. S. *Coord. Chem. Rev.* **2009**, *253*, 2891–2911.
- (12) (a) Xiang, S. C.; Zhou, W.; Zhang, Z. J.; Green, M. A.; Liu, Y.; Chen, B. *Angew. Chem., Int. Ed.* **2010**, *49*, 4615–4618; *Angew. Chem.* **2010**, *122*, 4719–4722. (b) Xiang, S. C.; Zhou, W.; Gallegos, J. M.; Liu, Y.; Chen, B. *J. Am. Chem. Soc.* **2009**, *131*, 12415–12419.
- (13) (a) Kreno, L. E.; Leong, K.; Farha, O. K.; Allendorf, M.; Van Duyne, R. P.; Hupp, J. T. *Chem. Rev.* **2012**, *112*, 1105–1125. (b) Hu, Z.; Deibert, B. J.; Li, J. *Chem. Soc. Rev.* **2014**, *43*, 5815–5840. (c) Mallick, A.; Garai, B.; Addicoat, M. A.; Petkov, P. S.; Heine, T.; Banerjee, R. *Chem. Sci.* **2015**, *6*, 1420–1425.
- (14) (a) Ramaswamy, P.; Wong, N. E.; Shimizu, G. K. H. *Chem. Soc. Rev.* **2014**, *43*, 5913–5932. (b) Ye, Y. X.; Zhang, L. Q.; Peng, Q. F.; Wang, G. E.; Shen, Y. C.; Li, Z. Y.; Wang, L. H.; Ma, X. L.; Chen, Q. H.; Zhang, Z. J.; Xiang, S. C. *J. Am. Chem. Soc.* **2015**, *137*, 913–918. (c) Aiyappa, H. B.; Saha, S.; Wadge, P.; Banerjee, R.; Kurungot, S. *Chem. Sci.* **2015**, *6*, 603–607.
- (15) (a) Liu, J.; Chen, L.; Cui, H.; Zhang, J.; Zhang, L.; Su, C. Y. *Chem. Soc. Rev.* **2014**, *43*, 6011–6061. (b) Lin, Z. J.; Lü, J.; Hong, M.; Cao, R. *Chem. Soc. Rev.* **2014**, *43*, 5867–5895.
- (16) Zhang, Z.; Yao, Z. Z.; Xiang, S.; Chen, B. *Energy Environ. Sci.* **2014**, *7*, 2868–2899.
- (17) (a) Gao, W. Y.; Cai, R.; Meng, L.; Wojtas, L.; Zhou, W.; Yildirim, T.; Shi, X.; Ma, S. *Chem. Commun.* **2013**, *49*, 10516–10518. (b) Ma, S.; Zhou, H. C. *J. Am. Chem. Soc.* **2006**, *128*, 11734–11735.
- (18) (a) Nelson, A. P.; Farha, O. K. K.; Mulfort, L.; Hupp, J. T. *J. Am. Chem. Soc.* **2009**, *131*, 458–460. (b) Ma, L.; Jin, A.; Xie, Z.; Lin, W. *Angew. Chem., Int. Ed.* **2009**, *48*, 9905–9908; *Angew. Chem.* **2009**, *121*, 10089–10092. (c) Park, H. J.; Lim, D. W.; Yang, W. S.; Oh, T. R.; Suh, M. P. *Chem. - Eur. J.* **2011**, *17*, 7251–7260.
- (19) Tan, Y. X.; He, Y. P.; Zhang, J. *Inorg. Chem.* **2012**, *51*, 9649–9654.
- (20) Lin, Z. J.; Liu, T. F.; Huang, Y. B.; Lü, J.; Cao, R. *Chem. - Eur. J.* **2012**, *18*, 7896–7902.
- (21) Jenkins, H. D. B.; Roobottom, H. K.; Passmore, J.; Glasser, L. *Inorg. Chem.* **1999**, *38*, 3609–3620.
- (22) (a) Naik, A. D.; Marchand-Brynaer, J.; Garcia, Y. *Synthesis* **2008**, *2008* (1), 149–154. (b) Chen, D. M.; Shi, W.; Cheng, P. *Chem. Commun.* **2015**, *51*, 370–372. (c) Wang, L. H.; Ye, Y. X.; Zhang, L. Q.; Chen, Q. H.; Ma, X. L.; Zhang, Z. J.; Xiang, S. C. *Inorg. Chem. Commun.* **2015**, *60*, 19–22.
- (23) (a) O’koye, I. P.; Benham, M.; Thomas, K. M. *Langmuir* **1997**, *13*, 4054–4059. (b) Xiang, S. C.; Zhang, Z. J.; Zhao, C. G.; Hong, K.; Zhao, X.; Ding, D. R.; Xie, M. H.; Wu, C. D.; Das, M. C.; Gill, R.; Thomas, K. M.; Chen, B. L.; Nat. *Nat. Commun.* **2011**, *2*, 204–210. (c) Zhang, Z. J.; Xiang, S. C.; Hong, K. L.; Das, M. C.; Arman, H. D.; Garcia, M.; Mondal, J. U.; Thomas, K. M.; Chen, B. L. *Inorg. Chem.* **2012**, *51*, 4947–4953. (d) Shen, Y. C.; Li, Z. Y.; Wang, L. H.; Ye, Y. X.; Liu, Q.; Ma, X. L.; Chen, Q. H.; Zhang, Z. J.; Xiang, S. C. *J. Mater. Chem. A* **2015**, *3*, 593–599. (e) Chen, Y.; Li, Z. Y.; Liu, Q.; Shen, Y. C.; Wu, X. Z.; Xu, D. D.; Ma, X. L.; Wang, L. H.; Chen, Q. H.; Zhang, Z. J.; Xiang, S. C. *Cryst. Growth Des.* **2015**, *15*, 3847–3852.
- (24) (a) Chang, H.; Wu, Z. X. *Ind. Eng. Chem. Res.* **2009**, *48*, 4466–4473. (b) Liu, J.; Tian, J.; Thallapally, P. K.; McGrail, B. P. *J. Phys. Chem. C* **2012**, *116*, 9575–9581.
- (25) (a) Sheldrick, G. M. *Acta Crystallogr., Sect. A: Found. Crystallogr.* **2008**, *64*, 112–122. (b) Dolomanov, A. V.; Bourhis, L. J.; Gildea, R. J.; Howard, J. A. K.; Puschmann, H. *J. Appl. Crystallogr.* **2009**, *42*, 339–341.
- (26) Sarkisov, L.; Harrison, A. *Mol. Simul.* **2011**, *37*, 1248–1257.
- (27) Spek, A. L. *J. Appl. Crystallogr.* **2003**, *36*, 7–13.
- (28) (a) Blatov, V. A.; Shevchenko, A. P.; Proserpio, D. M. *Cryst. Growth Des.* **2014**, *14*, 3576–3586. (b) Zhan, C. H.; Wang, F.; Kang, Y.; Zhang, J. *Inorg. Chem.* **2012**, *51*, 523–530. (c) Qin, Y. Y.; Ding, Q. R.; Yang, E.; Kang, Y.; Zhang, L.; Yao, Y. G. *Inorg. Chem. Commun.* **2015**, *56*, 83–86.
- (29) (a) Ammer, J.; Nolte, C.; Karaghiosoff, K.; Thallmair, S.; Mayer, P.; de Vivie-Riedle, R.; Mayr, H. *Chem. - Eur. J.* **2013**, *19*, 14612–14630. (b) Huang, W.; Wang, L.; Tanaka, H.; Ogawa, T. *Eur. J. Inorg. Chem.* **2009**, *2009*, 1321–1330. (c) Du, X.; Fan, R.; Wang, X.; Qiang, L.; Wang, P.; Gao, S.; Zhang, H.; Yang, Y.; Wang, Y. *Cryst. Growth Des.* **2015**, *15*, 2402–2412. (d) Park, K. M.; Lee, J.; Kang, Y. *Acta Cryst. E* **2015**, *71*, 354–356.
- (30) Jiang, Z. Q.; Jiang, G. Y.; Wang, F.; Zhao, Z.; Zhang, J. *Chem. - Eur. J.* **2012**, *18*, 10525–10529.
- (31) (a) Jia, J. T.; Sun, F. X.; Fang, Q. R.; Liang, X. Q.; Cai, K.; Bian, Z.; Zhao, H. J.; Gao, L. X.; Zhu, G. S. *Chem. Commun.* **2011**, *47*, 9167–9169. (b) Seo, J.; Chun, H. *Eur. J. Inorg. Chem.* **2009**, *2009*, 4946–4949. (c) Qin, J. S.; Du, D. Y.; Li, W. L.; Zhang, J. P.; Li, S. L.; Su, Z. M.; Wang, X. L.; Xu, Q.; Shao, K. Z.; Lan, Y. Q. *Chem. Sci.* **2012**, *3*, 2114–2118. (d) Li, S. L.; Lan, Y. Q.; Sakurai, H.; Xu, Q. *Chem. - Eur. J.* **2012**, *18*, 16302–16309.
- (32) Zhu, Y.; Murali, S.; Stoller, M. D.; Ganesh, K. J.; Cai, W.; Ferreira, P. J.; Pirkle, A.; Wallace, R. M.; Cychosz, K. A.; Thommes, M.; Su, D.; Stach, E. A.; Ruoff, S. *Science* **2011**, *332*, 1537–1541.
- (33) Chickos, J. S.; Acree, W. E. *J. Phys. Chem. Ref. Data* **2003**, *32*, 519–878.
- (34) Liao, P. Q.; Chen, H.; Zhou, D. D.; Liu, S. Y.; He, C. T.; Rui, Z.; Ji, H.; Zhang, J. P.; Chen, X. M. *Energy Environ. Sci.* **2015**, *8*, 1011–1016.
- (35) Millward, A. R.; Yaghi, O. M. *J. Am. Chem. Soc.* **2005**, *127*, 17998–17999.
- (36) Xiang, S. C.; He, Y. B.; Zhang, Z. J.; Wu, H.; Zhou, W.; Krishna, R.; Chen, B. L. *Nat. Commun.* **2012**, *3*, 954–962.
- (37) Nugent, P.; Belmabkhout, Y.; Burd, S. D.; Cairns, A. J.; Luebke, R.; Forrest, K.; Pham, T.; Ma, S.; Space, B.; Wojtas, L.; Eddaoudi, M.; Zaworotko, M. J. *Nature* **2013**, *495*, 80–84.
- (38) Nugent, P. S.; Rhodus, V. L.; Pham, T.; Forrest, K.; Wojtas, L.; Space, B.; Zaworotko, M. J. *J. Am. Chem. Soc.* **2013**, *135*, 10950–10953.
- (39) An, J.; Geib, S. J.; Rosi, N. L. *J. Am. Chem. Soc.* **2010**, *132*, 38–39.
- (40) McDonald, T. M.; Lee, W. R.; Mason, J. A.; Wiers, B. M.; Hong, C. S.; Long, J. R. *J. Am. Chem. Soc.* **2012**, *134*, 7056–7065.
- (41) McDonald, T. M.; D’Alessandro, D. M.; Krishna, R.; Long, J. R. *Chem. Sci.* **2011**, *2*, 2022–2028.
- (42) Caskey, S. R.; Wong-Foy, A. G.; Matzger, A. J. *J. Am. Chem. Soc.* **2008**, *130*, 10870–10871.
- (43) *CRC Handbook of Chemistry and Physics*, 74th ed.; Chemical Rubber Publishing Company: Boca Raton, Florida, 1993.

- (44) Nguyen, P. T. K.; Nguyen, H. T. D.; Pham, H. Q.; Kim, J.; Cordova, K. E.; Furukawa, H. *Inorg. Chem.* **2015**, *54*, 10065–10072.
- (45) Fracaroli, A. M.; Furukawa, H.; Suzuki, M.; Dodd, M.; Okajima, S.; Gandara, F.; Reimer, J. A.; Yaghi, O. M. *J. Am. Chem. Soc.* **2014**, *136*, 8863–8866.
- (46) Montoro, C.; García, E.; Calero, S.; Pérez-Fernández, M. A.; López, A. L.; Barea, E.; Navarro, J. A. R. *J. Mater. Chem.* **2012**, *22*, 10155–10158.
- (47) (a) Zhang, J. P.; Chen, X. M. *J. Am. Chem. Soc.* **2009**, *131*, 5516–5521. (b) Vaidyanathan, R.; Iremonger, S. S.; Shimizu, G. K. H.; Boyd, P. G.; Alavi, S.; Woo, T. K. *Science* **2010**, *330*, 650–653. (c) Liao, P. Q.; Zhou, D. D.; Zhu, A. X.; Jiang, L.; Lin, R. B.; Zhang, J. P.; Chen, X. M. *J. Am. Chem. Soc.* **2012**, *134*, 17380–17383. (d) Plonka, A. M.; Banerjee, D.; Woerner, W. R.; Zhang, Z.; Nijem, N.; Chabal, Y. J.; Li, J.; Parise, J. B. *Angew. Chem., Int. Ed.* **2013**, *52*, 1692–1695; *Angew. Chem.* **2013**, *125*, 1736–1739. (e) Lin, J. B.; Xue, W.; Zhang, J. P.; Chen, X. M. *Chem. Commun.* **2011**, *47*, 926–928. (f) Du, M.; Li, C. P.; Chen, M.; Ge, Z. W.; Wang, X.; Wang, L.; Liu, C. S. *J. Am. Chem. Soc.* **2014**, *136*, 10906–10909. (g) Hu, X. L.; Gong, Q. H.; Zhong, R. L.; Wang, X. L.; Qin, C.; Wang, H.; Li, J.; Shao, K. Z.; Su, Z. M. *Chem. - Eur. J.* **2015**, *21*, 7238–7244.
- (48) (a) Yazaydin, A. O.; Benin, A. I.; Faheem, S. A.; Jakubczak, P.; Low, J. J.; Willis, R. R.; Snurr, R. Q. *Chem. Mater.* **2009**, *21*, 1425–1430. (b) Poloni, R.; Smit, B.; Neaton, J. B. *J. Am. Chem. Soc.* **2012**, *134*, 6714–6719.
- (49) Drisdell, W. S.; Poloni, R.; McDonald, T. M.; Long, J. R.; Smit, B.; Neaton, J. B.; Prendergast, D.; Kortright, J. B. *J. Am. Chem. Soc.* **2013**, *135*, 18183–18190.
- (50) (a) Wriedt, M.; Sculley, J. P.; Yakovenko, A. A.; Ma, Y.; Halder, G. J.; Balbuena, P. B.; Zhou, H. C. *Angew. Chem., Int. Ed.* **2012**, *51*, 9804–9808; *Angew. Chem.* **2012**, *124*, 9942–9946. (b) Chen, L. J.; Mowat, J. P. S.; Fairen-Jimenez, D.; Morrison, C. A.; Thompson, S. P.; Wright, P. A.; Düren, T. *J. Am. Chem. Soc.* **2013**, *135*, 15763–15773. (c) Hamon, L.; Llewellyn, P. L.; Devic, T.; Ghoufi, A.; Clet, G.; Guillermin, V.; Pirngruber, G. D.; Maurin, G.; Serre, C.; Driver, G.; van Beek, W.; Jolimaître, E.; Vimont, A.; Daturi, M.; Férey, G. *J. Am. Chem. Soc.* **2009**, *131*, 17490–17499.